Cement and Concrete Research 39 (2009) 1111–1121

Contents lists available at ScienceDirect

Cement and Concrete Research

journal homepage: http://ees.elsevier.com/CEMCON/default.asp

Physical and microstructural aspects of sulfate attack on ordinary and limestone blended Portland cements

Thomas Schmidt [a,*], Barbara Lothenbach [a], Michael Romer [a,c], Jürg Neuenschwander [a], Karen Scrivener [b]

[a] Empa, Swiss Federal Laboratories for Materials Testing and Research, 8600 Dübendorf, Switzerland
[b] EPFL, Laboratory of Construction Materials, 1015 Lausanne, Switzerland
[c] Holcim Group Support Ltd, 5113 Holderbank, Switzerland

ARTICLE INFO

Article history:
Received 15 November 2008
Accepted 9 August 2009

Keywords:
Sulfate attack
Ettringite
Gypsum
Thaumasite
Temperature
Thermodynamic modelling

ABSTRACT

The consequences of external sulfate attack were investigated by traditional test methods, i.e. length and mass change, as well as by a newly developed, surface sensitive ultrasonic method, using Leaky Rayleigh waves (1 MHz). The macroscopic changes are discussed and compared with thermodynamic calculations and microstructural findings (SEM/EDS). The results show that the main impact of limestone additions on resistance to sulfate degradation are physical — i.e. addition of a few percent in Portland cement reduces the porosity and increases the resistance of Portland cement systems to sulfate; but higher addition of 25% increase porosity and lower resistance to sulfate. The kinetics of degradation were dramatically affected by the solution concentration (4 or 44 g Na_2SO_4/l) and the higher concentration also resulted in the formation of gypsum, which did not occur at the low concentration. However the pattern of cracking was similar in both cases and it appears that gypsum precipitates opportunistically in pre-formed cracks so it is not considered as making a significant contribution to the degradation. At 8 °C limited formation of thaumasite occurred in the surface region of the samples made from cement with limestone additions. This thaumasite formation led to loss of cohesion of the paste and loss of material from the surface of the samples. However thaumasite formation was always preceded by expansion and cracking of the samples due to ettringite formation and given the very slow kinetics of thaumasite formation it was probably facilitated by the opening up of the structure due to ettringite induced cracking.
The expansion of the samples showed a steady stage, followed by a rapidly accelerating stage, with destruction of the samples. The onset of the rapidly accelerating stage occurred when the thickness of the cracked surface layer reached about 1–1.5 mm–10–15% of the total specimen thickness (10 mm).

Contents

1. Introduction

The degradation of concrete due to ingress of sulfate ions from the environment — so called "sulfate attack" plays an important role in the

* Corresponding author. Tel.: +41 58 850 57 80; fax: +41 58 850 55 71.
E-mail address: thomas.schmidt@holcim.com (T. Schmidt).

0008-8846/$ – see front matter.
doi:10.1016/j.cemconres.2009.08.005

durability of certain structures. Damage due to sulfate interaction can result in the cracking and softening, with loss of strength of the concrete. The role in such damage of the precipitation of certain sulfate phases such as ettringite ($3CaO \cdot Al_2O_3 \cdot 3CaSO_4 \cdot 32H_2O$), gypsum ($CaSO_4 \cdot 2H_2O$) and thaumasite ($CaSiO_3 \cdot CaCO_3 \cdot CaSO_4 \cdot 15H_2O$) and the effect of internal carbonate such as limestone filler in cement is still not understood in detail.

The formation of secondary sulfate phases influences the microstructure of cementitious materials. Changes between the surface and the core regions of the affected structures have been studied and can be directly related to the uptake of sulfate and leaching [1–3]. The observed expansion is often attributed to the precipitation of secondary sulfate phases but no clear evidence was found linking expansion to e.g. the amount of secondary ettringite formed as different physical and chemical effects often overlap [4,5]. Various different theories exist regarding the mechanisms of expansion, e.g. increase in solid volume [6], topochemical reactions [7], swelling [8] or crystal growth [9] but often field and laboratory observations do not match. Gollop and Taylor [10] concluded that expansion was not a direct and immediate consequence of ettringite formation, but could be a delayed and possibly indirect consequence of it. More recent theories support the idea that crystallisation pressure develops in nanometric pores of the cement paste within weeks, producing the initial tensile stress and subsequently expansion of the matrix as suggested by Scherer [11]. It seems to agree very well with the macroscopic observations. Santhanam et al. [12] found that gypsum and ettringite can both contribute to expansion especially in Portland cements with high C_3S contents. Brown and Taylor [13] concluded that there is no linear relationship between the amount of ettringite formed and the observed expansion.

Many investigations of sulfate attack under laboratory conditions use high sulfate concentrations to accelerate physical and microstructural changes in the samples within short times. In the presence of high sulfate concentrations, gypsum is often formed besides ettringite, whereas under field conditions gypsum is rarely observed under field conditions where moderate or low sulfate concentrations are present [10,14–16].

Due to economical and ecological reasons, increasing amounts of limestone are blended with clinker during grinding of cement. Currently blended cements are available with up to 35 wt.% of limestone filler replacing the Portland cement clinker, although such cements are not allowed for use in environments where sulfate attack is possible. In some cases limestone additions have been regarded as an inert component in the cement [17,18]. However, it is now recognised [19] that a certain amount of the limestone (up to around 5%) reacts to give calcium alumino carbonate phases and monocarbonate is formed as the stable AFm phase instead of monosulfate [20,21]. The latter is resulting in a larger volume of hydrates and more aluminate is initially bound as ettringite which might chemically increase sulfate resistance. Beside that the higher volume of hydrates physically lowers the porosity. In the present paper the influence of limestone addition, and temperature on the physical and microstructural properties of a Portland cement mortars subject to sulfate solutions of different concentrations are investigated. The classical measurements of expansion and mass loss are compared with an innovative ultrasonic technique using Leaky Rayleigh waves to probe the topmost layer of the samples as described by Neuenschwander et al. [22].

The macroscopic changes are compared to the development of phases and damage in the microstructure. The phase changes observed experimentally are compared with those predicted from thermodynamic calculations.

2. Materials and methods

2.1. Laboratory cement and mortar samples

Three laboratory cements prepared from industrial Portland clinker were used for the experiments. Pure analytical gypsum was used to adjust the sulfate content to $SO_3 = 2.9$ wt.% for the 100% clinker cement, P0. To study the effect of limestone the clinker and gypsum were then blended with 5 or 25% of ground natural limestone: P5 and P25. The chemical composition of the materials as given in Table 1 was analysed by X-ray fluorescence (XRF, Philips PW 2400), sulfur and carbonate with a LECO C/S analyzer, and free lime according to Franke [23].

Mortars slabs $40 \times 160 \times 230$ mm^3 were fabricated according to EN 196-1 with a water/binder ratio of 0.5. These were cured for 28 days in saturated limewater ($Ca(OH)_2$, pH ≈ 12.5) at 20 °C. After curing, thin prisms were cut from the slabs to a size of $10 \times 40 \times 160$ mm^3. These prisms were sealed on their ends and plug gages were glued to these ends. The prisms were immersed in solutions of 4 g/l and 44 g/l Na_2SO_4 and in saturated lime solutions at 8 and 20 °C. The liquid/solid–volume ratio of the batches was 4 to 1. For all conditions five samples were prepared. The sulfate solutions were changed after 7, 14, 28, 56, 91, 180, 270 and 365 days.

The porosity was measured on the 28 days mortar samples according to Swiss standard SIA 162-1 [24], in which, the porosity was derived from the difference in mass of the water saturated sample to the dried sample. Thereby, the values for the total porosity were obtained from the mass change up to 105 °C; the air pores were obtained from the mass difference after 7 days vacuum saturation; the capillary pores were received from saturated samples dried at 50 °C to constant weight. Finally the gel porosity was calculated from the mass difference of samples dried at 105 °C and samples dried at 50 °C to constant weight. This classification was made according to the Swiss standard mentioned above.

Table 1
Composition of the laboratory cements including gypsum and limestone filler used.

	OPC[a]	Limestone[a]
Chemical analysis [g/100 g]		
CaO	63.7	55.9
SiO_2	20.1	0.05
Al_2O_3	4.4	0.10
Fe_2O_3	2.7	0.02
CaO (free)	0.85	<0.01
MgO	1.6	0.16
K_2O	0.86	<0.01
Na_2O	0.15	<0.01
CO_2	0.20	43.7
SO_3	2.90	<0.01
$K_2O_{soluble}$[b]	0.72	n.d.
$Na_2O_{soluble}$[b]	0.06	n.d.
Ignition loss	1.2	43.7
Blaine surface area [m^2/kg]	350	570

	P0	P5	P25
Calculated normative phase composition [g/100 g]			
Alite	63	59	47
Belite	10	10	8
Aluminate	7	7	5
Ferrite	8	8	7
CaO (free)[c]	0.9	0.8	0.6
$CaCO_3$[c]	0.4	5.4	25
$CaSO_4 \cdot 2H_2O$[c]	4.7	4.5	3.5
K_2SO_4[b]	1.3	1.3	1.0
Na_2SO_4[b]	0.1	0.1	0.1
Present as solid solution in the clinker phases			
K_2O[c]	0.14	0.13	0.10
Na_2O[c]	0.09	0.09	0.07
MgO[c]	1.6	1.5	1.2
SO_3[c]	0.03	0.03	0.02

[a] XRF data corrected for loss of ignition.
[b] Readily soluble alkalis calculated from the concentrations of alkalis measured in the solution after 5 min agitation at a *w/c* of 10; present as alkali sulfates.
[c] Calculated from the chemical analysis or TGA.

The mass and length of the specimens were recorded after 7, 14, 28, 56, 91, 180, 270 and 365 days. In addition, the velocity of Leaky Rayleigh waves was determined to investigate changes in the density of the surface of the mortar samples as described in Neuenschwander et al. [22]. The velocity of the Leaky Rayleigh wave c_{LR} is the average value of three different line scans using an immersion technique with low frequency probes (1 MHz) at the specific Leaky Rayleigh angle θ_{LR}. The response of this surface wave is sensitive to the top layer ($\leq$2 mm) of the samples (for more details see Neuenschwander et al. [22]).

The microstructure of the mortar samples was examined by scanning electron microscopy SEM (Philips ESEM FEG XL 30) using backscattered electron images and energy dispersive X-ray spectroscopy (EDS). Sample preparation involved drying, pressure impregnation with epoxy resin, cutting, polishing and coating with carbon. The chemical analysis using EDS was done with a Li/Si crystal detector and an accelerating voltage of 15 kV. The sulfate uptake was determined on polished samples as the SO_3 content by mass of cement paste using window frames (100 × 100 µm) at defined depths from the core to the surface regions.

To analyse the mineralogical composition of the hydrated cement paste before exposure to sodium sulfate solution, cement paste samples were prepared at a *w/c* of 0.4 and cured for 56 days in saturated limewater at 20 °C. The cement paste samples were crushed, washed in acetone, dried at 40 °C and analysed by XRD and TGA. TGA/DTG was carried out in open vessels in N_2 on about 10 mg of powdered cement paste at 20 °C/min up to 980 °C. The X-ray diffraction (XRD) analyses were performed on a PANalytical X'Pert PRO system using CuKα radiation.

2.2. Thermodynamic modelling

Thermodynamic modelling was carried out using the Gibbs free energy minimization program GEMS [25]. GEMS is a broad-purpose geochemical modelling code which computes equilibrium phase assemblage and speciation in a complex chemical system from its total bulk elemental composition. Chemical interactions involving solids, solid solutions, and aqueous electrolyte are considered simultaneously. The speciation of the dissolved species as well as the kind and amount of solids precipitated are calculated.

The thermodynamic data for aqueous species, gaseous phases as well as for many solids were taken from the PSI-GEMS thermodynamic database [26,27]. Solubility products for cement minerals including ettringite, different AFm phases, hydrogarnet, C–S–H and hydrotalcite were taken from the recent compilation of Lothenbach et al. [28] (cemdata07), the solubility of thaumasite from Schmidt et al. [29]. The extent of reaction of the clinker phases was calculated according to Lothenbach and Winnefeld [30] resulting in an overall degree of hydration of about 82% after 28 days. For the small amount of ferrite reacted, the formation of an ideal solid solution between Al- and Fe-containing analogues has been assumed. Thus, the expressions ettringite, monocarbonate, monosulfate, hemicarbonate or hydrotalcite in this paper all refer to the solid solution between the Al- and Fe-containing analogues. To describe the composition of C–S–H a model based on two concurrent solid solution between jennite ($C_{1.7}SH_{2.1}$) and tobermorite ($C_{0.83}SH_{1.3}$) and between tobermorite and SiO_2 was used (for details see [30]).

3. Results and discussion

3.1. Characterisation of hydrated mortar samples before sulfate interaction

The qualitative results of the mineralogical analysis of the cement pastes are shown in Table 2. Before exposure to sulfate solutions, mortar and paste samples were hydrated in saturated lime solutions.

Table 2
Summary of investigated mortar samples immersed in Na_2SO_4 solution at a given temperature and sulfate concentration; C–S–H and calcite in samples with 5 and 25% limestone present in the samples as analysed by SEM/EDS.

Sample		Affected surface	Unaltered core
30 g SO_4^{2-}/l after 56 days			
8 °C	P0	Gypsum, ettringite	Portlandite, monosulfate, *ettringite*
	P5	Gypsum, ettringite, *thaumasite*	Portlandite, monocarbonate, *ettringite*
	P25	Gypsum, ettringite, *thaumasite*	Portlandite, monocarbonate, *ettringite*
20 °C	P0	Gypsum, ettringite	Portlandite, monosulfate, *ettringite*
	P5	Gypsum, ettringite	Portlandite, monocarbonate, *ettringite*
	P25	Gypsum, ettringite, *thaumasite*	Portlandite, monocarbonate, *ettringite*
3 g SO_4^{2-}/l after 56 days			
20 °C	P0	*Gypsum*, ettringite	Portlandite, monosulfate, *ettringite*
	P5	*Gypsum*, ettringite	Portlandite, monocarbonate, *ettringite*
	P25	*Gypsum*, ettringite	Portlandite, monocarbonate, *ettringite*

Italic = small amounts.

The XRD data of the paste sample P0 showed that after 56 days besides some unhydrated clinker, mainly portlandite, ettringite as well as monosulfate were present as the main hydrates [29]. The EDS analysis of the P0 mortar samples showed the same phase assemblage for the hydrated, unaltered core of the sample (Table 2). Similarly P5 and P25, which contain 5% and 25% of limestone, unhydrated clinker, portlandite, and ettringite were found to be present after 56 days of hydration. However, instead of monosulfate, calcite and monocarbonate were identified, again both in the cement paste [29], as well as in the unaltered core of the mortar sample (see unaltered core data in Table 2).

This stabilisation of monocarbonate rather than monosulfate in the presence of calcite indirectly stabilises ettringite as there is proportionately more sulfate to alumina after formation of the monocarbonate. This observation is in agreement with thermodynamic calculations [20,21] as well as with experimental observations in different Portland cements [19,20,31]. This stabilisation of monocarbonate and ettringite in the presence of calcium carbonate leads to an increase of the volume of the hydrated phases at the same degree of hydration of the clinker component leading to a decrease in relative porosity of about 0.5% [20,21]. This agrees with the experimentally determined trends in capillary porosity (Table 3) which decreased slightly from 11.5 to 10% (±1%) respectively for P0 and P5 indicating small differences. The replacement of a higher fraction of cement by limestone, however, leads to an increase in capillary porosity: For P25 a capillary porosity of 14.5% (±1%) was measured; XRD and TGA indicate a similar degree of hydration. This increase of porosity with high replacement of limestone has been noted previously [14] and corresponds to a decrease in the amount of reactive clinker capable of filling space with hydrates.

3.2. Expansion, mass change and surface density

Figs. 1 and 2 show the expansion and mass changes for the 3 mortars at the two temperatures and two solution concentrations. At

Table 3
Summary of porosity obtained from mortar samples after 28 days of curing in limewater at 20 °C according to Swiss standard SIA 162-1 [24].

Sample	Porosity in vol.%		
	P0	P5	P25
Gel pores	4.4	5.3	3.3
Capillary pores	11.5	10.0	14.5
Air pores	1.0	1.2	3.0
Total	16.9	16.5	20.8

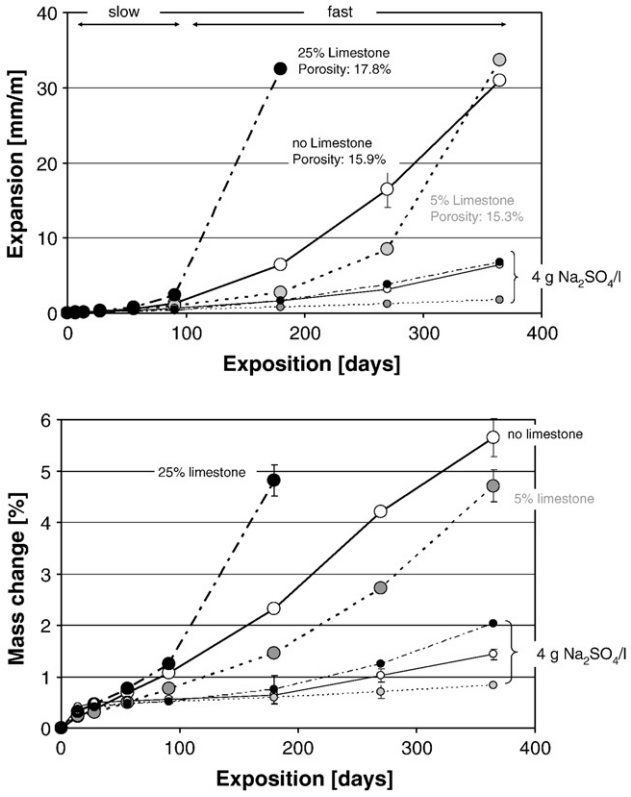

Fig. 1. Expansion and mass change of mortar samples immersed at 20 °C in 44 g (large circles) and 4 g (small circles) Na_2SO_4/l solution. The measured porosity (sum of gel and capillary pores) before sulfate interaction is given according to the limestone filler content of the binder.

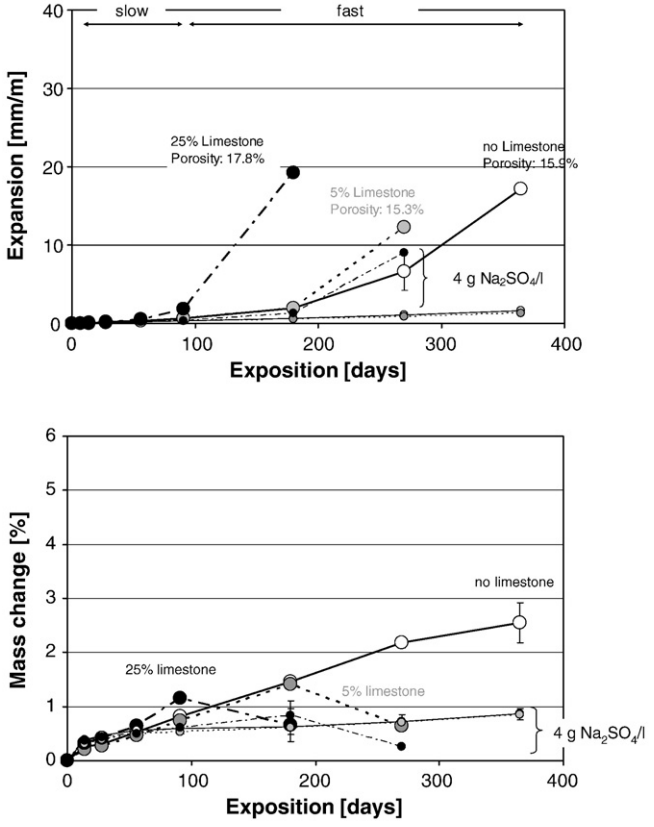

Fig. 2. Expansion and mass change of OPC mortar samples immersed in 44 g (large circles) and 4 g (small circles) Na_2SO_4/l solution at 8 °C. The measured porosity (sum of gel and capillary pores) before sulfate interaction is given according to the limestone filler content of the binder.

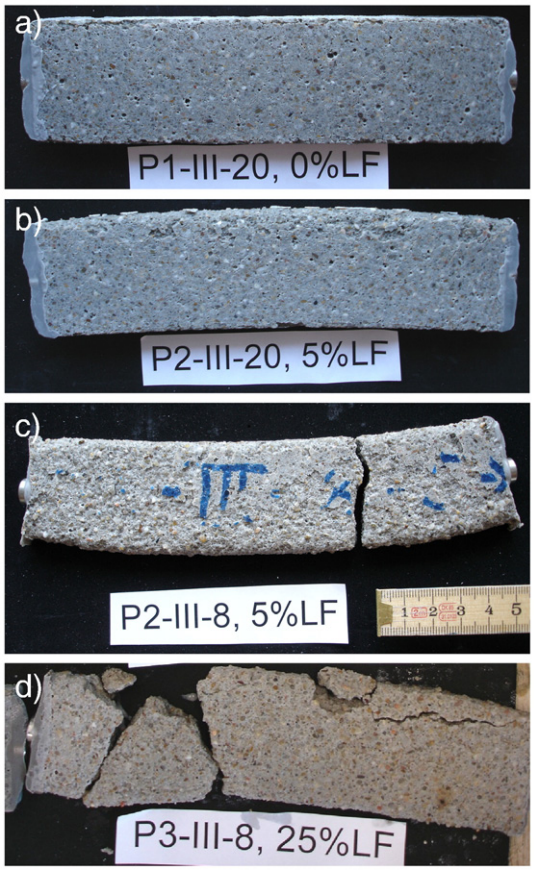

Fig. 3. OPC mortar samples containing a) 0% at 20 °C; b), c) 5% at 8 °C and 20 °C both 365 days, d) 25% limestone addition after 180 days at 8 °C all immersed in 44 g Na_2SO_4/l.

20 °C and high sulfate concentration in solution (44 g Na_2SO_4/l) all three mortars undergo catastrophic expansion by one year. The impact of the limestone addition on the kinetics of the expansion is clear. The sample P25 with 25% limestone is the most porous and starts to expand dramatically after 90 days and has fractured by 180 days of sulfate exposure, Fig. 3d. The mortar with 0% limestone (P0) also starts to expand rapidly after more than 90 days, but much less rapidly than the 25% (P25) sample and the 0% sample (P0) takes one year to reach the same degree of expansion as the 25% (P25) sample after 90 days. The sample with 5% limestone addition (P5) and the lowest porosity (15.3%) has a lower expansion than the sample without limestone addition (P0) at 180 and 270 days, but reaches a similar level of expansion after one year. After one year both the 0% and 5% samples remain intact, Fig. 3a, b although the 5% sample shows a pronounced curvature. The curvature seen in the 5% sample was often observed for samples which underwent large expansions. It is believed to be due to differences in the cement paste density and/or porosity at the top and bottom of the mortar samples due to fabrication. The towelled surface of the slab is always on the outer edge of the curve.

At the lower sulfate concentration in solution (4 g Na_2SO_4/l) the expansion of the samples is much less than at the higher sulfate concentration, but still significant by one year of exposure. Here it is seen that the samples with 0% and 25% limestone addition expand in a very similar way to about 7 mm/m after 1 year and with a sharply increasing rate from about 180 days. On the other hand the sample with 5% addition has only about 1 mm/m expansion at one year, with no sign of an increasing rate at this stage.

A characteristic of the expansion curves at both high and low sulfate concentration in solution is a period of steady slow expansion

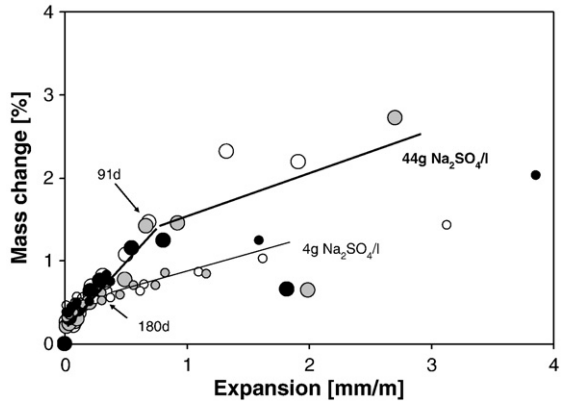

Fig. 4. Mass change versus expansion of OPC mortar samples immersed in 44 g (large circles) and 4 g (small circles) Na_2SO_4/l solution at 8 and 20 °C. The lines are intended as eye guides only. Black circles refer to P25, grey circles to P5 and white circles stand for P0 samples.

"progressive expansion style", followed by a sharply increasing rate of fast expansion "rapidly expansion style" (Figs. 1, 2). This change in behaviour is more apparent when the sample expansions are plotted against mass change, Fig. 4. It is seen that there is a strong increase of mass with expansion until a certain point, after which the relative mass gain becomes much less than the expansion. This point was observed to be after 91 days for high sulfate concentration and after 180 days for low sulfate concentration ion solution. This relationship suggested that the altered zone expands without cracking, with the uptake of water and sulfate, once the damage occurs the mass/expansion relationship is modified and an extended fast expansion and damage of the samples predominates.

At 8 °C and high sulfate concentration in solution (Fig. 2), the pattern of expansion is similar to that at 20 °C, with the 25% sample expanding catastrophically much earlier than the other two. However, in this case the expansion of the 5% limestone sample is somewhat faster than that of the 0% sample. A very different pattern is seen for the mass changes. The sample with 0% limestone addition shows a continuous mass gain (although lower than at 20 °C), while the mortars with 5% and 25% show a mass *loss* after the start of the rapidly increasing expansion. In these samples it could clearly be seen that this mass loss corresponds to softening and loss of the material starting from the surface of the samples, Fig. 3b, c. It was confirmed by other techniques discussed below that this mass loss corresponds to loss of material at the surface of the sample caused by the formation of thaumasite during sulfate exposure. At the lower sulfate concentration in solution (4 g Na_2SO_4/l), and 8 °C, the expansion and mass gain of the 0% and 5% samples are very low and hardly significant. However, even at the lower sulfate concentration, the highly porous sample with 25% limestone addition shows signs of damaging expansion at 270 days, with corresponding mass loss, Fig. 2.

The similarity of the expansive behaviour at 8 and 20 °C strongly implies that the same mechanism is occurring at both temperatures — independent of the formation of thaumasite. The formation of thaumasite is limited to the surface for samples which have already severely expanded, where it leads to dramatic loss of cohesion and disintegration in this surface region, Figs. 3b, c. Its precipitation, however leads to expansion. The mass loss and expansion phenomena caused by thaumasite formation might overlap and can not clearly be seen.

The changes in the relative Rayleigh wave velocity are shown in Fig. 5. This ultrasonic method allows the degradation process of the topmost layer of the samples surface (1–2 mm) [22] to be followed. Thereby, the signal is not affected by the unchanged bulk of the samples. An increase in the relative Rayleigh velocity c_{LR} indicates a densification of the surface while a decrease correlates with a lower

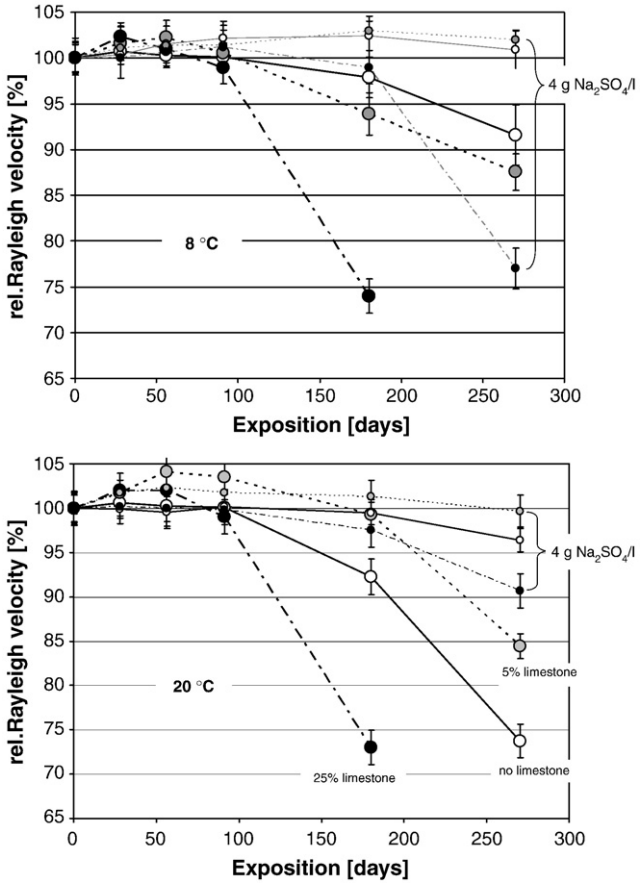

Fig. 5. Relative Rayleigh wave velocity c_{LR} of OPC mortar samples immersed in 44 g (large circles) and 4 g (small circles) Na_2SO_4/l solution at 8 and 20 °C according to the limestone filler content of the binder.

surface density. The relative Rayleigh velocity increased initially for the samples stored in Na_2SO_4 solutions as well as in the samples stored in saturated limewater [32]. This initial increase is caused by a densification of the microstructure as hydration continues and by the formation of new hydrate phases during sulfate interaction. After this initial densification there is a distinct drop of the relative Rayleigh velocity c_{LR} corresponding to the first desintegration of the microstructure. Overall the changes in relative Rayleigh velocity c_{LR} correspond very closely to the expansion measurements and do not seem to give any earlier indication of degradation. Perhaps this is not surprising in this case where the mortar prisms are so thin (10 mm) so that changes at the surface dominate their behaviour. In this case the greater simplicity and precision of the expansion measurements mean that there appears to be little advantage to the more complex Leaky Rayleigh velocity technique, however the later technique may be useful for larger prisms, where the unaltered bulk has a more important restraining effect on the degraded surface.

It is also interesting to note that, despite its sensitivity to changes at the surface, the technique does not indicate any major difference in behaviour between the samples exposed at 20 and 8 °C. This again indicates that thaumasite formation is the final step in the degradation process, occurring only after detrimental expansion and damage brought about by other mechanisms.

3.3. Thermodynamic modelling and experimental data

In a previous paper [29] we presented in more detail the thermodynamic changes predicted for samples subjected to increasing amounts of sodium sulfate in solution and compared this to the experimental changes observed for small pieces of cement pastes,

made from the same cements as discussed here. Thermodynamically it was shown that, when subject to increasing amounts of sulfate, first all the available alumina reacts to form ettringite. Then, in the presence of more sulfate, and if a source of carbonate is present, thaumasite should form. Thermodynamically there is a relatively small difference in the amount of thaumasite predicted to form at 8 and 20 °C–26 and 25 wt.% respectively for the 5% limestone addition and 68 and 59 wt.% for the 25% addition. The experimental study however showed that temperature had a major impact on the kinetics of thaumasite formation. At both temperatures the rate of formation was slow, with only a small fraction of the thermodynamically stable amount having formed after 9 months of immersion of the paste fragments in solution. At 8 °C around 1–1.5% formed in the 5% limestone addition paste and around 2% in the 25% addition paste after 9 months, in the two solutions equivalent to the addition of 10 and 20% of sulfate by weight of cement. At 20 °C only 0.3–0.5% of thaumasite was detected in the 5 and 25% addition pastes immersed in the solution with the highest sulfate additions (eq. 20% by wt cement). Furthermore as the kinetics of thaumasite formation were so slow, gypsum formed as a metastable product at the highest sulfate concentrations.

To study the thermodynamic changes expected due to the ingression of Na_2SO_4 into the mortar sample, the phase assemblages at various ratios Na_2SO_4 solution/mortar were calculated to simulate the condition of the surface of the sample being in contact with a large amount of Na_2SO_4 solution while the core of the sample is not or hardly affected (Figs. 6, 7). Such a modelling approach has the advantage that the calculations are very fast and flexible as no transport equations have to be considered, but has the disadvantage that the calculated data relate neither to time nor to distance. However, these calculations are an easily adaptable tool to calculate the sequence of phase assemblages to be encountered during a sulfate test.

Fig. 6 shows the simulated impact of the external solution concentration on the phase changes. The changes are shown for the cement with 5% limestone addition, but were generally similar for the other cements. For short term exposure to sulfate solutions of a few weeks the formation of thaumasite will be negligible [15,16] and so is suppressed in the calculation.

In the presence of 5% limestone, thermodynamic modelling predicts in the hydrated core of the mortar sample the presence of C–S–H, portlandite, hydrotalcite, calcite, monocarbonate and ettringite (Fig. 6), which agrees with the experimental observations (Fig. 8, Table 2). Upon ingression of Na_2SO_4 solution, monocarbonate (AFm) and a fraction of the portlandite convert to ettringite and calcite until all aluminium (and iron) available is present as AFt. Closer to the sample surface, the remaining portlandite is predicted to dissolve first. At the surface in contact with Na_2SO_4 solution, the sample is leached;

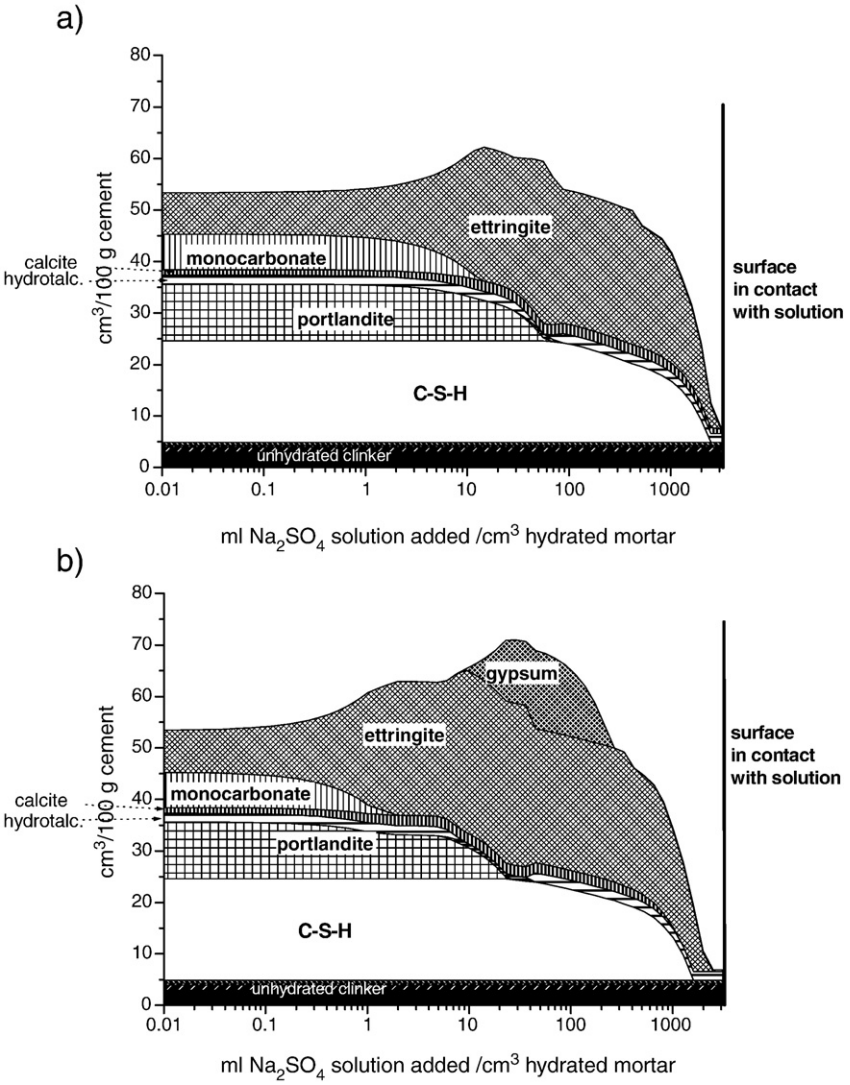

Fig. 6. Calculated phase assemblage of the P5 mortar sample immersed in a) 4 and b) 44 g/l Na_2SO_4 solutions excluding thaumasite due to kinetic reasons.

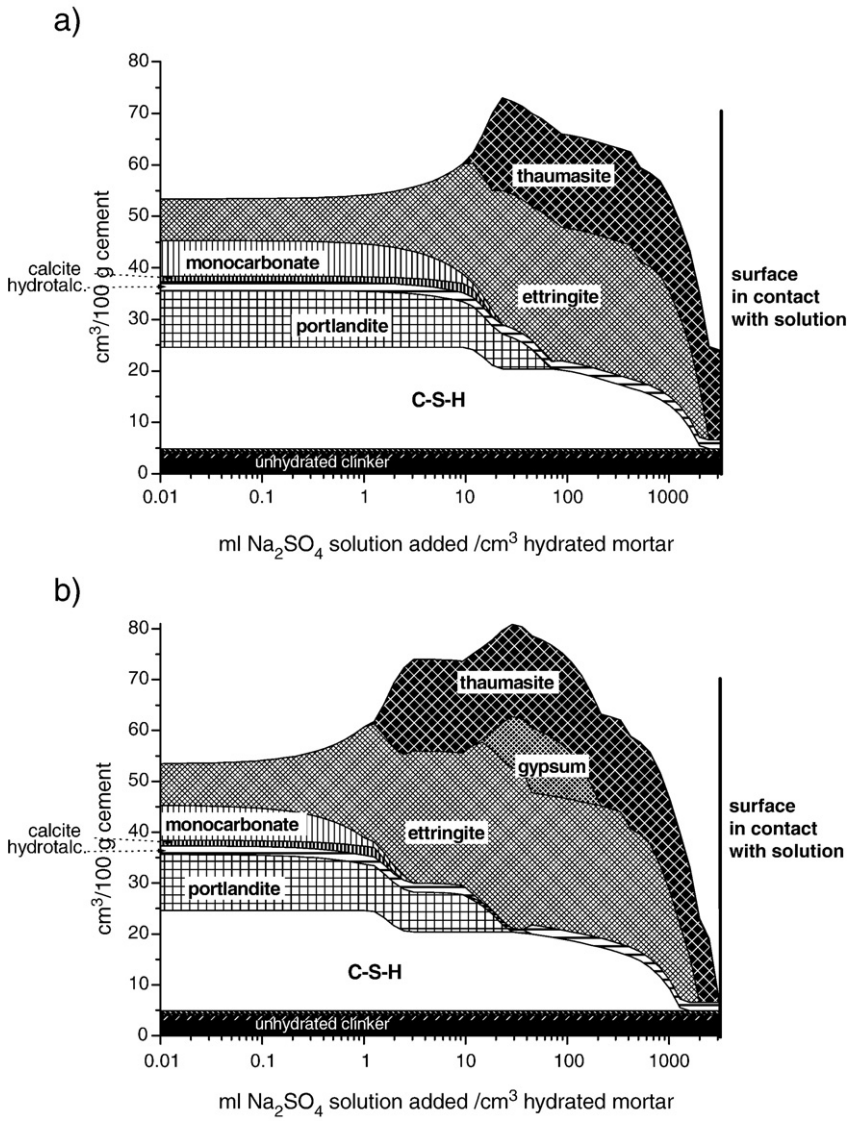

Fig. 7. Calculated phase assemblage of the P5 mortar sample immersed in a) 4 and b) 44 g/l Na_2SO_4 solutions including thaumasite in the database.

calcium and alkalies dissolved from the cement paste into the Na_2SO_4 solution and the hydrate phases become unstable. This sequence as calculated by thermodynamic modelling agrees well with changes reported in the literature [29,33] as well as with our experimental observations discussed below (Table 2).

In the presence of 44 g/l Na_2SO_4, gypsum is predicted to precipitate until all portlandite is consumed (Fig. 6b), while in the presence of lower sulfate concentrations (4 g/l Na_2SO_4), no or only very little gypsum was calculated to form (Fig. 6a). This again agrees qualitatively with previous investigations [4,14,33] and experimental observations (Table 2). Thermodynamic modelling shows that in the presence of low sulfate concentrations, as can be expected under field conditions, no or only very little gypsum precipitates while in the presence of higher concentrations as generally used in tests, a significant amount of gypsum precipitates.

To consider the long term formation of thaumasite, the thermodynamic calculations were repeated allowing the precipitation of thaumasite for both for high (44 g/l) and low (4 g/l) concentrations of the Na_2SO_4 solution (Fig. 7). In addition to the phase assemblage calculated in the absence of thaumasite, the formation of significant quantities of thaumasite were calculated to form near the surface where the sulfate ingress. Even in this case, the calculations indicate that thaumasite starts to form *only after* all aluminium has reacted to form secondary ettringite [29,34] for both high and low Na_2SO_4 concentrations, i.e. thaumasite will form only after ettringite has formed. Experimentally, thaumasite was found to precipitate very slowly due to its slow reaction kinetics [28]. Also at low sulfate concentrations the formation of thaumasite is possible if enough sulfate has entered the sample with time which agrees to the previous findings [29,35].

3.4. Phase assemblage and microstructure

Fig. 8 shows the sulfate uptake in the paste as a function of depth and gives a qualitative idea of the phase changes as determined by X-ray diffraction of material scrapped from the surface and from micro-analyses points taken in the cement paste (C–S–H phase) [32]. The samples analysed were immersed in both high and low sulfate concentration in solutions for 56 days and for the samples immersed in the lower sulfate concentration in solution for 270 days. All the samples show the formation of zones of different phase assemblages corresponding to those predicted by the thermodynamic modelling (Figs. 6, 7) — i.e. moving from the unaltered core to the surface the AFm phases are progressively replaced by ettringite with partial depletion of the portlandite. At the higher sulfate concentration in solution there is a distinct formation of gypsum near the surface, giving a marked peak in

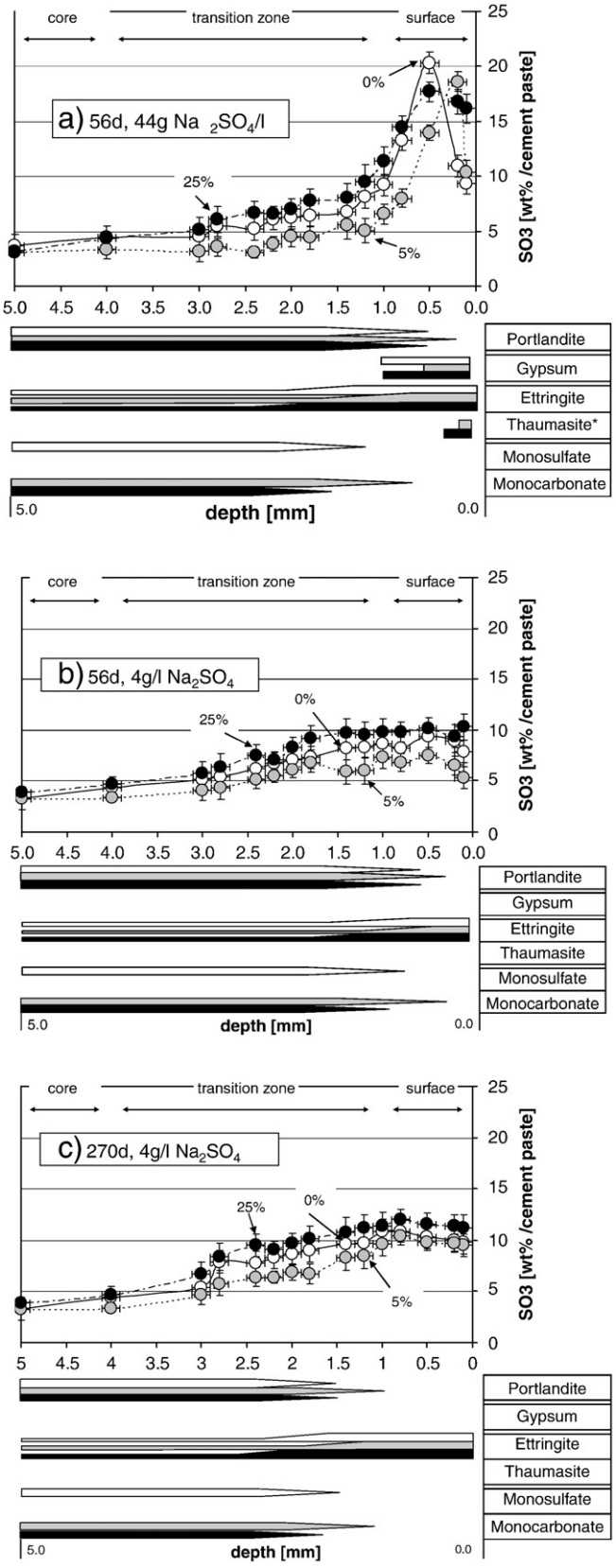

Fig. 8. Sulfate distribution in OPC mortar samples with up to 25% limestone addition immersed in high and low sulfate concentration in solution after a, b) 56 days and c) 270 days at 20 °C. (* = minor amounts at 8 °C).

sulfate content in the paste. At 8 °C at the high sulfate concentration in solution, in the presence of calcium carbonate (P5, P25), small amounts of thaumasite were found in the samples close to the surface (Fig. 8a).

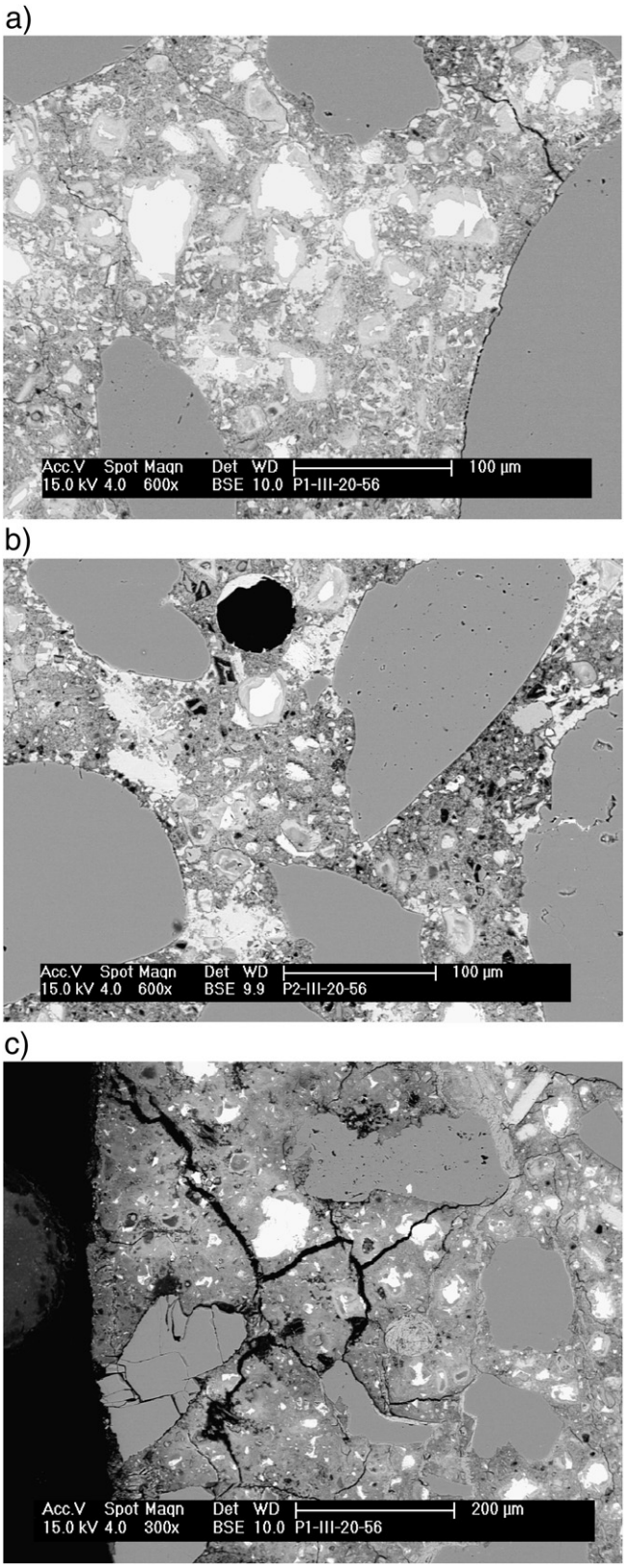

Fig. 9. BSE images of a) core- b) transition- and c) surface region of P0 mortar samples immersed in Na_2SO_4 solution for 56 days at 20 °C.

The sulfate profiles and depth of the zones reveal a systematic trend in the penetration depth of the sulfate for the different cement blends. In all cases the depth of penetration and the amount of sulfate at a given depth is highest for the samples made with the cement with 25% limestone addition (P25) followed by the sample with 0% addition (P0). The sample prepared with 5% addition of limestone (P5) show the lowest penetration of sulfate. This trend corresponds well with the trend in initial porosity report in Table 3 and with the pattern of expansion observed (Figs. 1, 2).

Fig. 9 shows low magnification images of three of the P0 mortar samples, with the corresponding zonations. With regard to evidence of expansion and damage all samples show the same characteristics:

- a core region characterised by a dense and compact microstructure and a good bonding between cement paste and aggregates (Fig. 9a);
- a transition zone (1.0–3.0 mm depth from surface) showed first signs of changes in the microstructure of the cement paste (Fig. 9b).
- a surface region (0–1.0 mm depth from surface) where the microstructure was characterised by crack formation between or around the aggregates (Fig. 9c). The cracks were either parallel or perpendicular to the sample surface and generally empty, except in the samples exposed at the high concentration where some cracks were filled with gypsum.

The microstructure of the surface zone, shares certain characteristics with samples which have undergone temperature induced internal sulfate attack (usually known as DEF, delayed ettringite formation) [5], in which cracks open up around the aggregate due to expansion in the paste, although the crack pattern is more complex in this case as there is also a gradient in the sulfate concentration from the surface to the interior. Therefore, it is proposed that the origin of expansion is the transformation of AFm phases (either monosulfate, in the case of P0 or monocarbonate in the cases of P5 and P25, Fig. 8), which are finely dispersed within the C–S–H phase. The micrographs 10, 11 provide further evidence for this, Fig. 10 shows ettringite precipitation in pores, which is believed to be non-expansive [36], while Fig. 11 shows inner product "C–S–H" which now contains a significant concentration of ettringite and is heavily cracked and deformed. In the "transition" zone a few cracks are observed from expanding still compact cement paste matrix (Fig. 11), but in the outer surface zone cracks open up around and between the aggregates (Fig. 10). This also illustrates quite well the physical mechanisms of the expansion towards the surface as mentioned below.

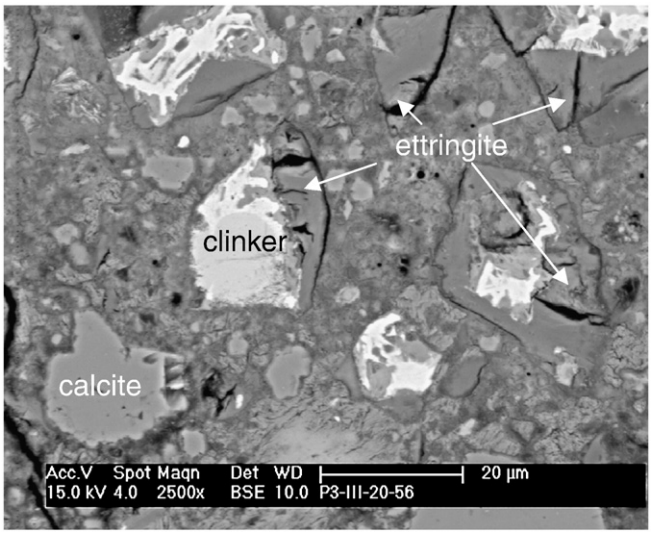

Fig. 11. SEM image of P25 mortar sample of the transition zone exposed to 44 g Na_2SO_4/l solution for 56 days at 20 °C.

It is proposed that degradation occurs due to the generation of expansive stresses in the paste component, which develop progressively from the surface. These expansive forces cause a macroscopic expansion of the sample, which at first expands progressively, but at a certain point, when the strength of the unaltered core is unable to withstand the forces from the expanding surface, a progressive mechanical failure of the sample starts with a corresponding rapidly increasing rate of expansion. The experimental observations support this theory as the depth of the heavily cracked surface layers reach about 1–1.5 mm in the samples which had reached the rapidly expanding stage, while it was much less for the samples still in the progressive expansion stage as mentioned above.

The formation of cracks around aggregates also opens up the microstructure to penetration of the sulfate solution. In most cases cracks were empty, but in the samples exposed to the high sulfate concentration some cracks contained gypsum (Fig. 12). The gypsum deposits often predominated as a "vein" of precipitates in cracks running subparallel to the surface, suggesting that their formation is favoured in the region where the extent of leaching is not too advanced. This also corresponds to the thermodynamic calculations where gypsum precipitated at high sulfate contents in the paste consuming part of the portlandite. However,

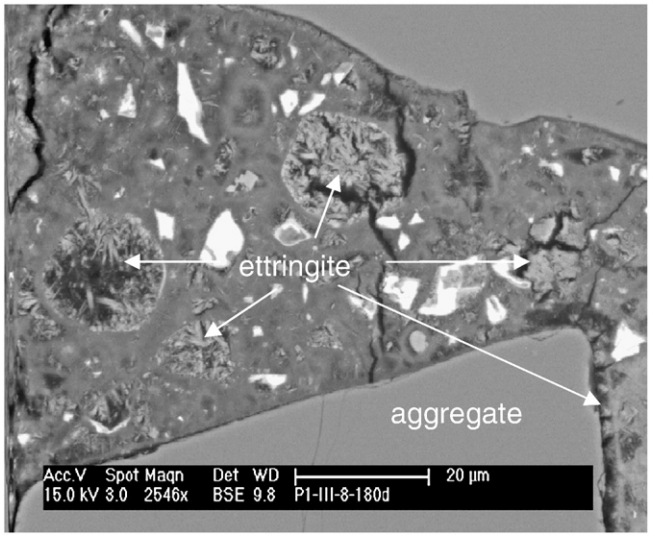

Fig. 10. SEM image of P0 mortar sample of surface region exposed to 44 g Na_2SO_4/l solution for 180 days at 8 °C.

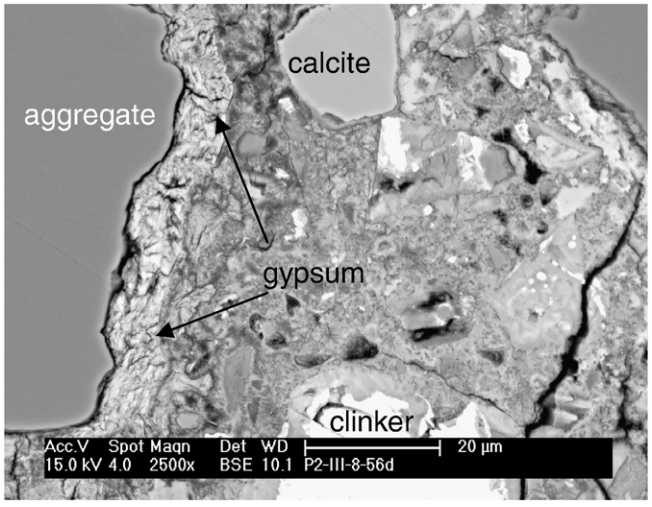

Fig. 12. SEM image of P5 mortar sample in the surface region at 0.5 mm depth exposed to 44 g Na_2SO_4/l solution for 56 days at 8 °C.

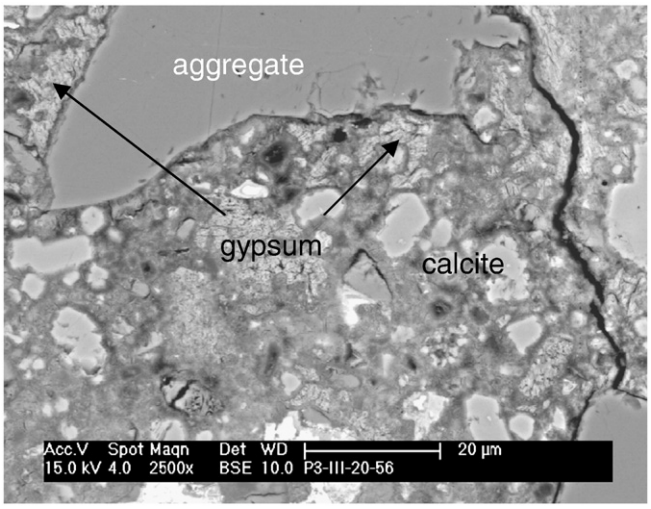

Fig. 13. SEM image of P25 mortar sample in the beginning of transition zone at 1 mm depth exposed to 44 g Na_2SO_4/l solution after 56 days at 20 °C.

it is important to note that deposits of gypsum were also found beneath this sub-surface vein, often replacing deposits of portlandite in the beginning of the interfacial transition zone, Fig. 13 (up to 1 mm). The fact that the progress of damage follows the same pattern, albeit with very different kinetics in the samples exposed to the high concentrations (where gypsum forms) and in those at the lower sulfate concentration (where no or only little gypsum is formed) indicate that the role of gypsum precipitation in the expansive process is to open up already existing cracks from ettringite formation. This fits the hypothesis that expansive forces are generated by the formation of phases in confined space [5] — i.e. ettringite from AFm within C–S–H phase of the cement paste. However, it is noted here that expansion due (probably) to gypsum formation has been observed in other samples, which contained most of the alumina present as ettringite before exposure to sulfate solutions. It appears that the transformation of microcrystalline portlandite to gypsum within the C–S–H can be the origin of expansion as analysed by Gollop and Taylor [10].

In the samples with limestone additions exposed at 8 °C, the presence of thaumasite in the region very close to the surface was confirmed (Fig. 14). The depth at which thaumasite occurred was

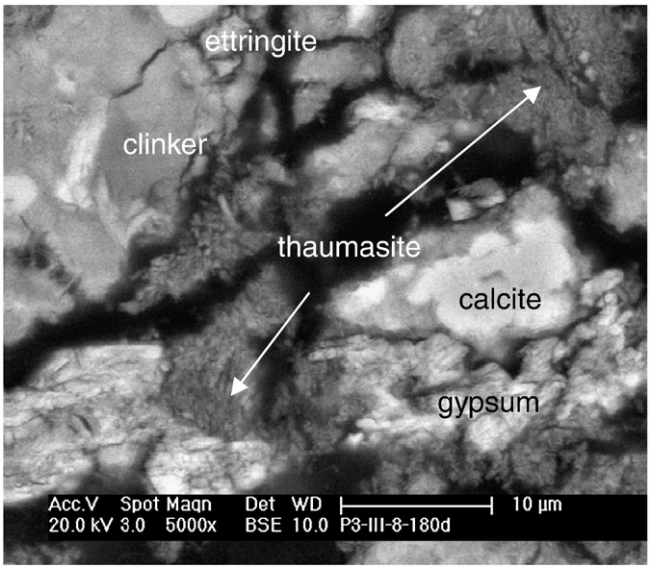

Fig. 14. SEM image of P25 mortar sample in surface region at 0.5 mm depth exposed to 44 g Na_2SO_4/l solution after 180 days at 8 °C.

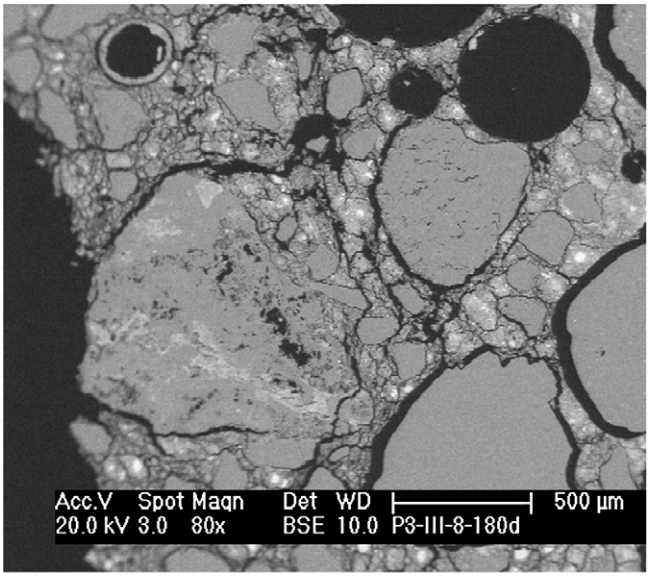

Fig. 15. SEM image of P25 mortar sample of surface region up to 2.0 mm depth exposed to 44 g Na_2SO_4/l solution after180 days at 8 °C.

always less than 0.5 mm. Furthermore the overall pattern of crack damage was very similar to that of the samples exposed at 20 °C where almost no thaumasite was formed. These observations lead to the conclusion that thaumasite formation is the final stage of sulfate attack and that, in the materials studied here, damaging expansion due to ettringite formation occurs first — opening up the microstructure (Fig. 15). When thaumasite formation then takes place it leads to a loss on cohesion of the cement paste and to a loss of material from the sample.

4. Conclusions

The impact of limestone additions on degradation in sulfate solutions are dominated by their impact on the cement paste porosity and on the rate of sulfate ingress. The addition of 5 wt.% limestone in Portland cement systems led to a decrease in sulfate uptake due to its lower initial capillary porosity. Especially at ambient temperatures (20 °C) the sulfate induced deterioration was reduced. In the case of 25 wt.% limestone addition the initial porosity was increased and the sulfate induced deterioration was accelerated. These observations indicate that the initial porosity (permeability) of the cement system influences sulfate interaction and the sulfate resistance.

Both monosulfate and monocarbonate AFm phases transform to ettringite in the presence of ingressing sulfate ions. As most of these AFm phases are finely intermixed with the C–S–H phase, the transformation within the confining environment of the C–S–H leads to the generation of expansive forces. As expansion occurs throughout the cement paste component, cracks open up around the aggregate particles.

Once the depth of the heavily cracked surface region evolves to a depth of about 1–1.5 mm, rapidly increasing and ultimately catastrophic expansion starts, which appear to be related to the point at which the strength of the unaltered core can no longer withstand the expansive forces at the surface. This may also be related to the development of cracks of critical length in the surface region, which can propagate through the sample.

When mortar samples are immersed in solutions of high sulfate concentration, gypsum may also form close to the surface. However it does not appear that this makes a significant contribution to the damage in these systems where ettringite expansion dominates.

Although it is predicted to be a thermodynamically stable phase at both 20 and 8 °C, significant formation of thaumasite was observed

only at the low temperature in the near surface regions, after extensive formation of gypsum. The formation of thaumasite leads to a loss of cohesion and softening of the surface region. Thaumasite was detected to form within the C–S–H phase of the cement paste consuming the available carbonate and sulfate. Thaumasite formation was associated with significant mass loss of the samples. Study of the damage evolution indicated that ettringite related expansion preceded thaumasite formation and indeed the opening up of the microstructure due to expansion may be a necessary precursor for the formation of thaumasite.

An ultrasound immersion technique using low frequency (1 MHz) and ultrasonic surface waves was successfully applied for the investigation of degradation processes on mortar samples. The measured Leaky Rayleigh wave allowed the sulfate degradation mechanisms specifically in the mortar samples surface to be followed without taking into account the unchanged core region. However for the thin prisms used here there seemed to be no advantage in sensitivity compared to expansion measurements.

Acknowledgements

The authors would like to thank L. Brunetti, W. Trindler, T. Lüthi, B. Ingold and E. Gallucci for their assistance in the experimental part of this study and F. Glasser, T. Matschei for insights in thermodynamic modelling. Special thanks to Cemsuisse, the association of the Swiss Cement Industry, for the financial support.

References

[1] J. Skalny, J. Marchand, I. Odler, Sulfate attack on concrete, Modern concrete technology, vol. 10, 2002, London.
[2] D. Bonen, M.D. Cohen, Magnesium sulfate attack on Portland cement paste — I. Microstructural analysis, Cem. Concr. Res. 22 (1992) 169–180.
[3] D. Bonen, M.D. Cohen, Magnesium sulfate attack on Portland cement paste — II. Chemical and mineralogical analyses, Cem. Concr. Res. 22 (1992) 707–718.
[4] D. Planel, J. Sercombe, P. Le Besop, F. Adenot, J.M. Torrenti, Long-term performance of cement paste during combined calcium leaching-sulfate attack: kinetics and size effect, Cem. Concr. Res. 36 (1) (2006) 137–143.
[5] H.F.W. Taylor, C. Famy, K.L. Scrivener, Delayed ettringite formation, Cem. Concr. Res. 31 (2001) 683–693.
[6] H.F.W Taylor, Sulfate reactions in concrete — microstructural and chemical aspects, Cement Technology (Ceramic Transactions), vol. 40, 1989, pp. 61–78, Westerville, OH.
[7] P.W. Brown, S. Badger, The distribution of bound sulfates and chlorides in concrete subjected to mixed NaCl, $MgSO_4$, Na_2SO_4 attack, Cem. Concr. Res. 30 (2000) 1535–1542.
[8] T. Thorvaldson, Chemical aspects of the durability of cement products, Proceedings of 3rd International Symposium on the Chemistry of Cement, Cement and Concrete Association, London, 1954.
[9] S. Diamond, Delayed ettringite formation — processes and problems, Cem. Concr. Res. 18 (3) (1996) 205–215.
[10] R. Gollop, H.F.W Taylor, Microstructural and microanalytical studies of sulfate attack, I. Ordinary Portland cement paste, Cem. Concr. Res. 22 (1992) 1027–1038.
[11] G.W. Scherer, Stress from crystalisation of salt, Cem. Concr. Res. 34 (9) (2004) 1613–1624.
[12] M. Santhanam, M.D. Cohen, J. Olek, Effects of gypsum formation on the performance of cement mortars during external sulfate attack, Cem. Concr. Res. 33 (2003) 325–332.
[13] P.W. Brown, H.F.W. Taylor, The Role of Ettringite in External Sulfate Attack. Materials of Science of Concrete: Sulfate Attack Mechanisms, special volume The American Ceramic Society 1998 73-97.
[14] E.F. Irassar, V.L. Bonavetti, M. Gonzalez, Microstructural study of sulfate attack on ordinary and limestone Portland cements at ambient temperature, Cem. Concr. Res. 33 (2003) 31–41.
[15] J. Marchand, E. Samson, Y. Maltais, J.J. Beaudoin, Theoretical analysis of the effect of weak sodium sulfate solutions on the durability of concrete, Cem. Concr. Compos. 24 (3–4) (2002) 317–329.
[16] F. Bellmann, B. Moser, J. Stark, Influence of sulfate solution concentration on the formation of gypsum in sulfate resistance test specimen, Cem. Concr. Res. 36 (2) (2006) 358–363.
[17] H. Uchikawa, S. Hanehara, H. Hirao, Influence of microstructure on the physical properties of concrete prepared by substituting mineral powder for part of fine aggregate, Cem. Concr. Res. 26 (1996) 101–111.
[18] T. Vuk, V. Tinta, R. Gabrovsek, V. Kaucic, The effects of limestone addition, clinker type and fineness on properties of Portland cement, Cem. Concr. Res. 31 (2001) 135–139.
[19] H. Kuzel, H. Pöllmann, Hydration of C_3A in the presence of $Ca(OH)_2$, $CaSO_4$*$2H_2O$ and $CaCO_3$, Cem. Concr. Res. 21 (1991) 885–895.
[20] B. Lothenbach, G. LeSaout, E. Gallucci, K.L. Scrivener, Influence of limestone on the hydration of Portland cements, Cem. Concr. Res. 38 (6) (2008) 848–860.
[21] T. Matschei, B. Lothenbach, F.P. Glasser, The role of calcium carbonate in cement hydration, Cem. Concr. Res. 37 (4) (2007) 551–558.
[22] J. Neuenschwander, Th. Schmidt, Th Lüthi, M. Romer, Leaky Rayleigh wave investigation on mortar samples, Ultrasonics 45 (1–4) (2006) 50–55.
[23] A. Franke, Bestimmung von Calciumoxid und Calciumhydroxid neben wasserfreiem und wasserhaltigem Calciumsilikat, Z. Aorg. allg. Chem. (247) (1941) 180–184.
[24] SN-505-162/1, Betonbau-Ergänzende Festlegungen, SIA, Zürich, 1989.
[25] D. Kulik, GEMS-PSI 2.2. 2007, available at http://gems.web.psi.ch/: PSI-Villigen, Switzerland.
[26] T. Thoenen, D. Kulik, Nagra/PSI chemical thermodynamic database 01/01 for the GEM-Selektor (V.2-PSI) geochemical modeling code, PSI, Villigen, 2003, http://les.web.psi.ch/Software/GEMS-PSI/doc/pdf/TM-44-03-04-web.pdf.
[27] W. Hummel, U. Berner, E. Curti, F.J. Pearson, Nagra/PSI Chemical Thermodynamic Data Base 01/01. 2002, USA, also published as Nagra Technical Report NTB 02-16, Wettingen, Switzerland: Universal Publishers/uPUBLISH.com. 565.
[28] B. Lothenbach, T. Matschei, G. Möschner, F.P. Glasser, Thermodynamic modelling of the effect of temperature on the hydration and porosity of Portland cement, Cem. Concr. Res. 38 (2008) 1–18.
[29] T. Schmidt, B. Lothenbach, M. Romer, K. Scrivener, D. Rentsch, R. Figi, A thermodynamic and experimental study of the conditions of thaumasite formation, Cem. Concr. Res. 38 (2008) 337–349.
[30] B. Lothenbach, F. Winnefeld, Thermodynamic modelling of the hydration of Portland cement, Cem. Concr. Res. 36 (2005) 209–226.
[31] V.L. Bonavetti, V.F. Rahhal, E.F. Irassar, Studies on the carboaluminate formation in limestone filler-blended cements, Cem. Concr. Res. 31 (2001) 853–859.
[32] T. Schmidt, Sulfate attack and the role of internal carbonate on the formation of thaumasite. Thesis EPFL No. 3853, Lausanne Switzerland, 2007.
[33] P. Le Bescop, C. Solet, External sulphate attack by ground water, experimental study on CEM I cement pastes, Revue européene de genie civil 10 (9) (2006) 1127–1145.
[34] E.F. Irassar, M.A. Bonavetti, M.A. Trezza, M. Gonzalez, Thaumasite formation in limestone filler cements exposed to sodium sulphate solution at 20 °C, Cem. Concr. Compos. 27 (2005) 77–84.
[35] D.W. Hobbs, Thaumasite sulfate attack in field and laboratory concretes: implications for specifications, Cem. Concr. Compos. 25 (8) (2003) 1195–1202.
[36] E.F. Irassar, V.L. Bonavetti, M. Gonzalez, Microstructural study of sulfate attack on ordinary and limestone Portland cements at ambient temperature, Cem. Concr. Res. 25 (4) (1995) 903–914.